Viscoelastic Response of Fibroblasts to Tension Transmitted through Adherens Junctions

G. Keith Ragsdale, John Phelps, and Katherine Luby-Phelps
Department of Physiology, The University of Texas Southwestern Medical School, Dallas, Texas 75235-9040 USA

ABSTRACT Cytoplasmic deformation was monitored by observing the displacements of 200-nm green fluorescent beads microinjected into the cytoplasm of Swiss 3T3 fibroblasts. We noted a novel protrusion of nonruffling cell margins that was accompanied by axial flow of beads and cytoplasmic vesicles as far as 50 μm behind the protruding plasma membrane. Fluorescent analog cytochemistry and immunofluorescence localization of F-actin, α-actinin, N-cadherin, and β-catenin showed that the protruding margins of deforming cells were mechanically coupled to neighboring cells by adherens junctions. Observations suggested that protrusion resulted from passive linear deformation in response to tensile stress exerted by centripetal contraction of the neighboring cell. The time dependence of cytoplasmic strain calculated from the displacements of beads and vesicles was fit quantitatively by a Kelvin-Voight model for a viscoelastic solid with a mean limiting strain of 0.58 and a mean strain rate of 4.3×10^{-3} s^{-1}. In rare instances, the deforming cell and its neighbor spontaneously became uncoupled, and recoil of the protruding margin was observed. The time dependence of strain during recoil also fit a Kelvin-Voight model with similar parameters, suggesting that the kinetics of deformation primarily reflect the mechanical properties of the deformed cell rather than the contractile properties of its neighbor. The existence of mechanical coupling between adjacent fibroblasts through adherens junctions and the viscoelastic responses of cells to tension transmitted directly from cell to cell are factors that must be taken into account to fully understand the role of fibroblasts in such biological processes as wound closure and extracellular matrix remodeling during tissue development.

INTRODUCTION

Many essential functions of differentiated cells depend on their ability to deform or to resist deformation. Epithelial cells resist mechanical stress to maintain the integrity of tissues and organs. Vascular endothelial cells withstand the high shear stresses arising from arterial blood flow as well as tangential stresses associated with the dilation and constriction of blood vessels. Locomotion and contraction of fibroblasts is required for wound healing and for remodeling of extracellular matrix during tissue development. Blood cells are deformed passively as they pass through the spleen or capillaries. Leukocytes and macrophages actively deform to invade tissue beds by ameboid locomotion or to engulf foreign particles. To understand in detail the mechanisms that account for any of these functions it is essential to characterize the mechanical properties of cells and how these properties are regulated.

The mechanical properties of cells have been studied by several methods, including micropipette aspiration, micromanipulation, and analysis of the response of ingested or implanted ferromagnetic particles to applied magnetic fields (Bizal et al., 1991; Elson, 1988; Felder and Elson, 1990; Sato et al., 1984; Zahalak et al., 1990). In some cases, particularly for erythrocytes and leukocytes, the results have been expressed in terms of quantitative viscoelastic models. In contrast, most studies involving single epithelial, endothelial, or fibroblast cells have been qualitative or comparative. Nevertheless, such studies make it clear that the mechanical properties of cells are modulated in response to intracellular or extracellular signals (Danowski and Harris, 1988; Hiramoto, 1990; Liu et al., 1987; Wang et al., 1993a,b) and suggest that cellular deformation can regulate cell growth and gene expression (Ingber et al., 1994).

Ingested polystyrene beads have been employed as visible markers of spontaneous cytoplasmic deformation in neutrophils (Simon and Schmid-Schonbein, 1990). A modification of this approach has allowed us to examine the mechanical properties of cytoplasm in single living fibroblasts. Swiss 3T3 (SW3T3) cells were microinjected with 200-nm green fluorescent beads as markers of cytoplasmic deformation and rhodamine-dextran as a marker of cytoplasmic volume. We observed that cells were often stretched by the spontaneous contraction of neighboring cells to which they were mechanically coupled through adherens junctions. Microinjection of fluorescent analogs of actin and α-actinin revealed that actin filament bundles run parallel to the axis of deformation, inserting into the adherens junctions at the cell margin (Fig. 1 *A*). Time lapse observation demonstrated that these bundles elongated as the cell was stretched. Using the injected beads as internal strain gauges, we found that stretching also was accompanied by significant deformation of the cytoplasm between filament bundles. The time dependence of cytoplasmic strain was consistent with a model in which the contracting cell exerts a constant stress on its neighbor and the neighbor responds as a Kelvin-Voight viscoelastic solid (Fig. 1 *B*). Assuming a value on the order of 10^4 dynes/cm^2 for the

Received for publication 22 August 1996 and in final form 5 August 1997.
Address reprint requests to Dr. Katherine Luby-Phelps, Department of Physiology, University of Texas SW Medical Center, 5323 Harry Hines Blvd., Dallas, TX 75235-9040. Tel.: 214-648-2190; Fax: 214-648-8685; E-mail: lubyphel@utsw.swmed.edu.

0006-3495/97/11/2798/11 $2.00

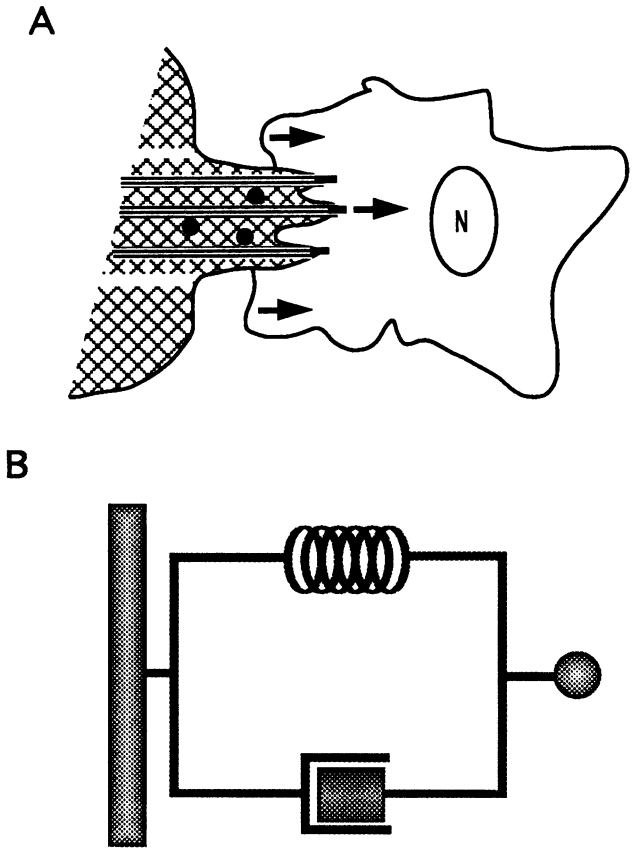

FIGURE 1 (*A*) Model for deformation of fibroblast cytoplasm. Beads or large vesicles (●) are depicted as trapped in a network of cytoskeletal filaments. The network is continuous with bundles of parallel actin filaments that insert into adherens junctions ([GRAPHIC]) between the cell on the left and its neighbor. As the neighbor contracts, the margin of the cell on the left is drawn out, the actin filament bundles elongate, and the network is deformed, leading to displacement of the entrapped beads and vesicles. Shear zones parallel to the axis of deformation are depicted as breaks in the network. (*B*) Diagram of a Kelvin-Voight viscoelastic solid showing an elastic element (spring) and a viscous element (dashpot) in parallel.

stress exerted by the contracting cell (see Discussion), the model predicts an elastic modulus of 1.7×10^4 dynes/cm^2 and a viscosity of 4×10^6 Poise for fibroblast cytoplasm. To our knowledge, these represent the first quantitative estimates of the bulk material properties of single fibroblasts. The importance of these data is enhanced by the fact that the measurements were made under noninvasive conditions while the cells were responding to mechanical stress of physiological origin.

MATERIALS AND METHODS

Cell culture

Swiss 3T3 fibroblasts (catalog item CCL-92, American Type Culture Collection, Rockville, MD) were plated on 40-mm round glass coverslips (Fisher Scientific, Pittsburgh, PA) and cultured as described (Provance et al., 1993). All experiments were performed on cells in Dulbecco's minimal essential medium (Gibco/BRL, Gaithersburg, MD) containing 10% bovine serum.

Fluorescent labeling of proteins

Actin was purified from rabbit muscle acetone powder as described (Spudich and Watt, 1971) and labeled on cysteine using iodoacetamido tetramethyl rhodamine (catalog item T-488, Molecular Probes, Eugene, OR) as described (DeBiasio et al., 1987). The dye-to-protein molar ratio of the adduct (AR-actin) was 0.8 using 7.6×10^4 as the molar extinction coefficient for rhodamine. α-Actinin was purified from chicken gizzard as described (Feramisco and Burridge, 1980) and labeled with iodoacetamido tetramethyl rhodamine as described (Meigs and Wang, 1986). The dye-to-protein molar ratio of the adduct (AR-α-actinin) was 0.4.

Microinjection and digital fluorescence imaging

Green fluorescent beads of 200 nm diameter with a net positive surface charge (L-5381, Molecular Probes) were diluted to 5.3×10^8 particles per ml in a solution of 10-kDa rhodamine-dextran (D-1824, Molecular Probes) at 1 mg/ml. The mixture was microinjected into living SW3T3 cells as described (Provance et al., 1993). For some experiments, AR-actin or AR-α-actinin was injected at a needle concentration of 2 or 5 mg/ml, respectively. After a 2–4 h recovery period, coverslips with injected cells were mounted in a modified Sykes-Moore chamber (Custom Scientific, Dallas, TX) and maintained at 37°C as described (Provance et al., 1993). Fluorescence was viewed with an Axiovert 135 microscope (Carl Zeiss, Thornwood, NY) with a 40× 1.3 NA or a 100× 1.3 NA lens and narrow bandpass fluorescein and rhodamine filter sets (Omega Optical, Brattleboro, VT). Digital images were acquired using a cooled Nu200 series CCD camera with a 14-bit Thompson chip (Photometrics, Tucson, AZ) and transferred to a Macintosh IIfx with 32 Mbytes RAM (Apple Computer, Cupertino, CA). For automated acquisition of time series, the microscope and camera shutters were controlled using BDS-Image v. 1.4.3 software (Oncor Image, Gaithersburg, MD). Background images were taken from regions of the coverslip with no injected cells. BDS-Image was used to process and enhance images as follows. Fluorescence images were background subtracted and then sharpened using a Laplacian filter. In some cases, the fluorescein and rhodamine images were registered and added together. For path-length determinations, regions of interest in the rhodamine-dextran images were selected interactively and mean fluorescence intensity was obtained using either BDS-Image or NIH-Image v. 1.55.

Immunofluorescence

Cells were fixed in 3.7% formaldehyde in 60 mM Pipes; 25 mM Hepes; 10 mM EGTA; 2 mM $MgCl_2$; pH 6.9 (PHEM) buffer at 37°C and processed for immunofluorescence as described (Provance et al., 1993). A monoclonal antibody to vinculin (catalog item V-9131) was purchased from Sigma Chemical Co. (St. Louis, MO). Monoclonal antibodies to paxillin (P13520) and β-catenin (C19220) were purchased from Transduction Labs (Lexington, KY). A mouse monoclonal antibody to N-cadherin was the generous gift of Dr. Margaret Wheelock, University of Toledo. Rhodamine-labeled goat anti-mouse IgG was used as the secondary antibody.

Particle tracking and morphometry

Green fluorescent beads were tracked by thresholding the stack of images for each time series and using NIH-Image to find the centroids of selected beads in each image of the stack.The x–y coordinates of the centroids of vesicles were estimated interactively from unthresholded images. The base of an extending column of cytoplasm was defined as a line perpendicular to the axis of extension, distal to which no axial movement of cytoplasmic markers was observed. The distance of each bead or vesicle from this baseline in the first image of the stack (L_o) was measured using NIH-

Image. Displacements (ΔL) were calculated from the series of x–y coordinates of the centroids using the distance formula. Strain was calculated as $\Delta L/L_o$. Mean square displacement for selected beads was also calculated and plotted against time using a program written in Labview graphical programming language (National Instruments, Austin, TX). Using DeltaGraph Pro v. 3.5 (DeltaPoint, Monterey, CA), curves were fit to the subset of data for which the relative error was $\leq 1\%$ (Qian et al., 1991).

Viscoelastic modeling

The equation describing the relationship between strain (ϵ) and time (t) for a Kelvin-Voight viscoelastic element (spring and dashpot in parallel) is

$$\epsilon = A(1 - e^{-kt}) \quad (1)$$

where A is the limiting strain (σ/E), k is the strain rate (E/η), σ is the applied stress, E is the elastic modulus of the material, and η is the viscosity of the material. However, our analysis was complicated by the fact that we did not know the actual zero time for most of our data sets. Equation 1 can be transformed to take this into account by including offsets for the strain and time:

$$\epsilon - \epsilon' = A(1 - Be^{kt}) \quad (2)$$

where B is $e^{-kt'}$, and ϵ' and t' are the strain and time offsets, respectively. The strain and time data for beads and vesicles in each stack were normalized to the first image in the stack. Plots of strain versus time were fit to Eq. 2 using DeltaGraph Pro v. 3.5 to obtain ϵ' and t'. Corrected data were replotted and fit to Eq. 1.

RESULTS

A novel protrusion of fibroblast cell margins is accompanied by cytoplasmic deformation

Green fluorescent beads (200 nm diameter) were microinjected into living SW3T3 fibroblasts as markers of cytoplasmic deformation. The beads were chosen to have a net positive surface charge, as it has been reported by a number of investigators that positively charged beads are not transported on microtubules and apparently undergo Brownian motion in the cytoplasm of injected cells (Beckerle, 1984; Geerts et al., 1987; Wadsworth, 1987). Rhodamine dextran (10 kDa) was coinjected with the beads to serve as a volume marker. Changes in cell shape and spontaneous displacements of the beads were observed by time lapse digital fluorescence microscopy as described in Materials and Methods.

In subconfluent cultures and in confluent monolayers that had been wounded by scraping off a thin strip of cells, the lateral margins of some cells were seen to protrude outward for as long as 15 min at a maximal velocity ~1.5 μm/min (Fig. 2). In contrast to the smoothly convex protrusions at the leading edge of migrating cells, these protruding margins had a dentate profile that changed little during the course of the protrusion. Protruding margins were further distinguished from leading edges in that organelles were not excluded and no cycles of protrusion and retraction were observed. Ruffles were never observed on the protruding margin, although other edges of the same cell did exhibit ruffling (Fig. 2 *A*).

Green fluorescent beads and dextran-excluding vesicles in the protruding cell were observed to flow along the axis of protrusion (Fig. 2 *D*). Axial flow generally extended for tens of microns behind the protruding margin of the cell. Shear zones in the cytoplasm were observed at the boundaries between the protrusion and flanking regions of the cell margin that remained fixed (Fig. 2, *D* and *E*). Single particle tracking showed that trajectories of beads within a column of flowing material were parabolic, consistent with convective flow (Qian et al., 1991). Trajectories of beads located beyond the shear zone were linear, consistent with Brownian motion (Fig. 2 *E*). In general, the transport of markers within the column of flowing cytoplasm was spatially coordinated: beads and vesicles as far as 10 μm apart across the axis of protrusion kept abreast of one another for the duration of protrusion. However, in close proximity to the shear zone a steeply decreasing gradient in velocity was observed (Fig. 2, *D* and *E*).

Protrusion is accompanied by elongation of actin filament bundles

BODIPY-phallacidin staining of cells that were fixed while protruding showed that bundles of actin filaments were aligned along the axis of protrusion, with the tips of the bundles running up into the projections at the protruding margin of the cell (not shown). A similar result was observed in living cells that had been microinjected with a functional fluorescent analog of actin (AR-actin; Fig. 3). Time lapse records of these cells revealed that the tips of the actin filament bundles translocated relative to the substratum along with the cell margin during protrusion. In cases where the fluorescence intensity varied segmentally along the bundle, it was observed that individual segments moved relative to fixed markers without changing length (Fig. 3, *C* and *D*). These observations suggested that the actin filament bundles elongate during protrusion.

To examine the apparent elongation of actin filament bundles in more detail, we microinjected cells with a functional fluorescent analog of α-actinin (AR-α-actinin). This analog generally decorated actin filament bundles along their length in a periodic pattern, as expected from reports in the literature (Feramisco, 1979; Meigs and Wang, 1986; Sanger et al., 1986). Along cell margins where neighboring cells contacted one another, the distal ends of the bundles appeared to be capped by intensely fluorescent accumulations of AR-α-actinin (Fig. 4). Within protruding regions, the α-actinin decoration of actin filament bundles was less intense and lacked well defined periodicity (Fig. 4, *A* and *B*). During protrusion, the spacing between foci of α-actinin decoration at the base of the protrusion increased progressively, and the fluorescent caps of α-actinin at the cell margin translocated in the direction of protrusion (Fig. 4, *C* and *D*).

Protruding cell margins are coupled to neighboring cells via adherens junctions

When cells undergoing lateral protrusion were observed by phase contrast or differential interference contrast micros-

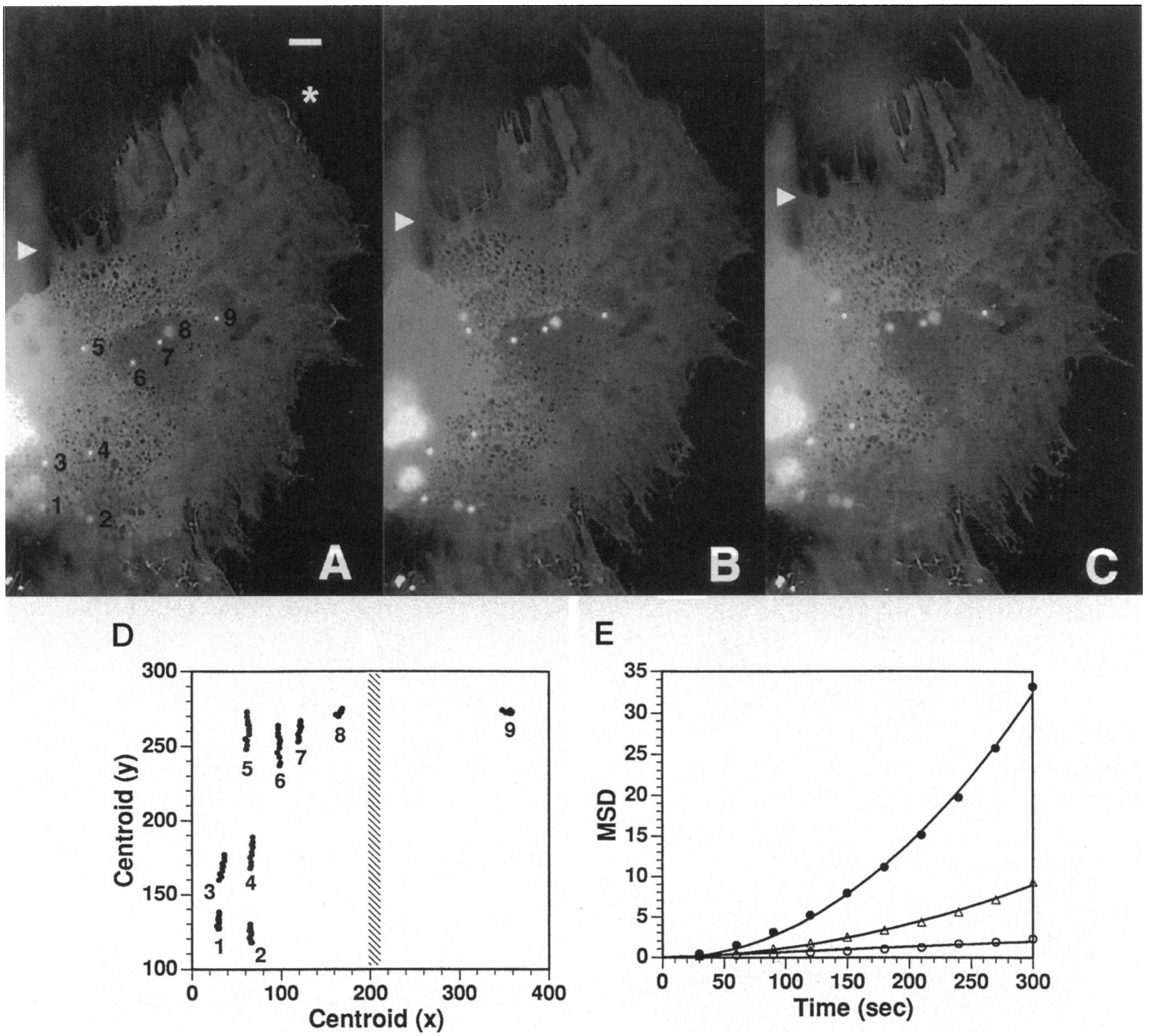

FIGURE 2 Lateral protrusion of cells is accompanied by flow of cytoplasmic markers. (*A–C*) Three images from a time series of a Swiss 3T3 cell undergoing lateral extension. The rhodamine-dextran image and green fluorescent bead image have been superimposed in each frame. (*A*) 0 min; (*B*) 3.5 min; (*C*) 6 min. The margin of the cell extended continuously at a maximal rate of 1.5 μm/min throughout the 12-min time sequence (*white arrowheads*). No ruffling was observed along the protruding cell margin, although ruffling was observed along other margins of the cell (*white asterisk*). Microinjected beads and endogenous organelles as far as 50 μm from the plasma membrane were translocated in the direction of protrusion while maintaining their relative positions across the axis of protrusion. (*D*) Paths of beads during lateral extension. Note that bead 9 does not appear to be translocated in the direction of extension, indicating a shear zone (*hatched line*) parallel to the axis of extension located between bead 7 and bead 9. (*E*) Mean square displacement (MSD) in square microns versus time in seconds for beads 7, 8, and 9. The plots for bead 7 (●) and bead 8 (△) are parabolic ($R^2 = 0.99$), consistent with convective flow. The plot for bead 9 (○) is linear ($R^2 = 0.97$), indicating its motion is Brownian. The velocity of bead 8 (0.6 μm/min) is much slower than that of bead 7 (1.14 μm/min), illustrating the gradient in transport velocity that was observed in close proximity with the shear zone. Bar in *A*, 5 μm.

copy, it could be seen that a protruding margin invariably overlapped the margin of a neighboring cell, even in sparsely seeded cultures. In cases where both the protruding cell and its neighbor had been microinjected with fluorescent markers, it was observed that the neighboring cell retracted or contracted centripetally as the protruding cell extended, suggesting that the protruding cell was passively deformed as a result of contractile stress exerted by its neighbor. Consistent with this idea, protrusion stopped when the neighboring cell was no longer visibly shortening.

The intimate contact between cells along the protruding margin, together with the localization of F-actin and α-actinin, suggested that the protruding cell and its neighbor might be mechanically coupled by means of adherens junctions. To test this hypothesis, we examined the localization of several junctional proteins. Cells were injected with a

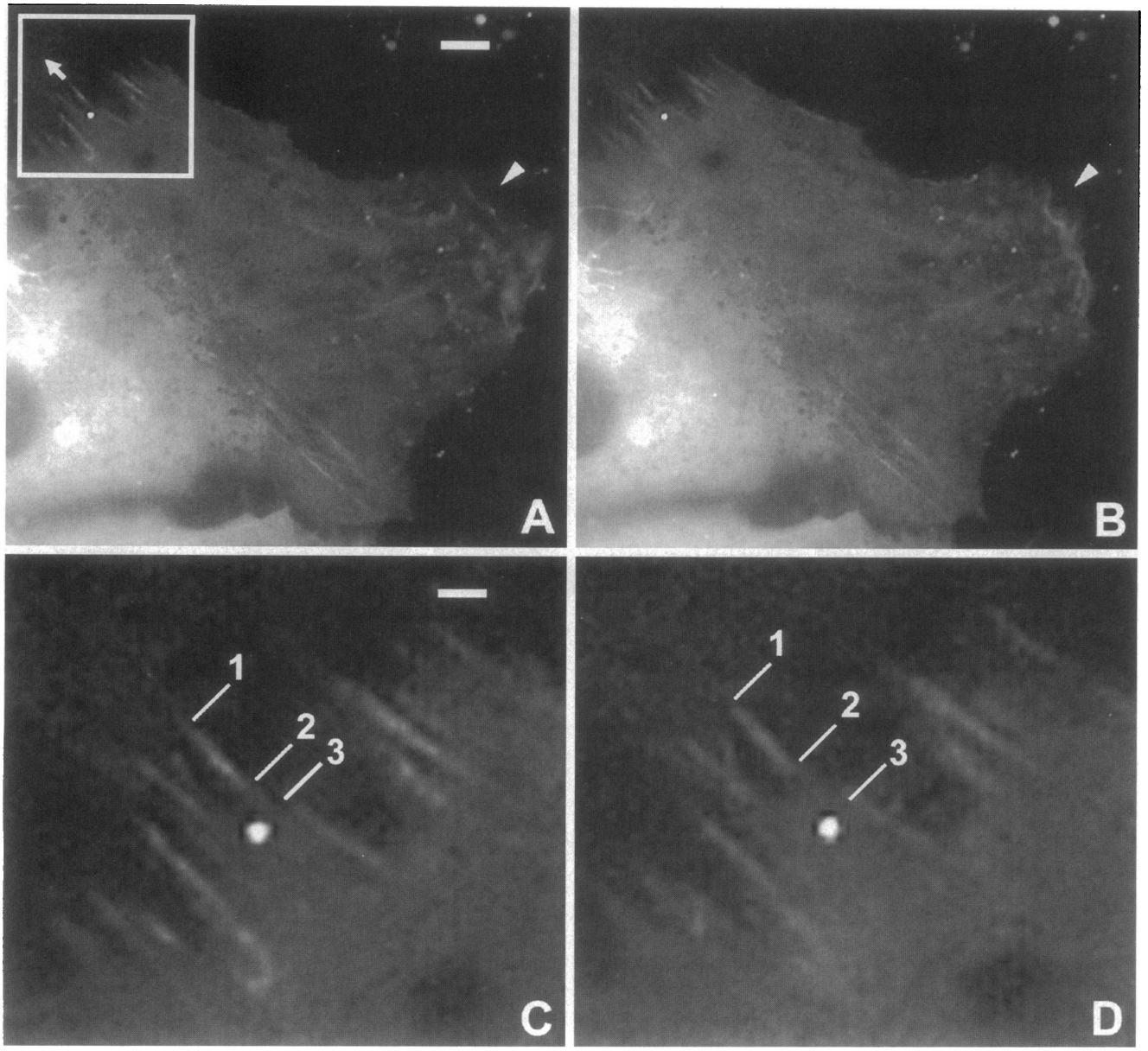

FIGURE 3 The tips of actin filament bundles at the cell margin translocate during protrusion. (*A*) and (*B*) Two images from a time series of a Swiss 3T3 cell undergoing protrusion in the direction indicated by the white arrow (*top left*). (*A*) and (*C*) 2 min; (*B*) and (*D*) 4 min. The cell has been microinjected with AR-actin, which incorporates into endogenous actin filament bundles. Filament bundles are aligned along the axis of extension with one end of the bundle running up into the tips of the projections at the protruding margin. (*C*) and (*D*) Enlargements of boxed region in *A*. A segment of increased fluorescence intensity along one of the bundles can be seen to translocate relative to a fixed marker without changing in length; 1 and 2 demarcate either end of the segment, and 3 demarcates the fixed marker. The distance between 1 and 2 remains constant, whereas the distances of 1 and 2 from 3 increase. Note the ruffling margin at the leading edge of this polarized cell (*A, arrowhead*). Bars, 5 μm (*A*) and 1.6 μm (*C*).

fixable fluorescein dextran (10 kDa) as a volume marker to allow relocation of specific cells after fixation and processing for immunofluorescence. Cultures were fixed immediately after acquiring a time series of a protruding cell, and immunofluorescence was carried out as described in Materials and Methods. We found that N-cadherin and β-catenin immunofluorescence was strongly co-localized in discrete, linear structures at the protruding cell margins of deforming cells (Fig. 5). This morphology is characteristic of adherens junctions. Vinculin and paxillin immunofluorescence was absent from the junctions, although these antigens were localized to focal contacts in the same cells (not shown).

Viscoelastic response of 3T3 fibroblasts

To characterize the cytoplasmic deformation during protrusion, we measured the displacements of bead and vesicle markers as described in Materials and Methods. Over any time interval, the linear displacement (ΔL) of each marker

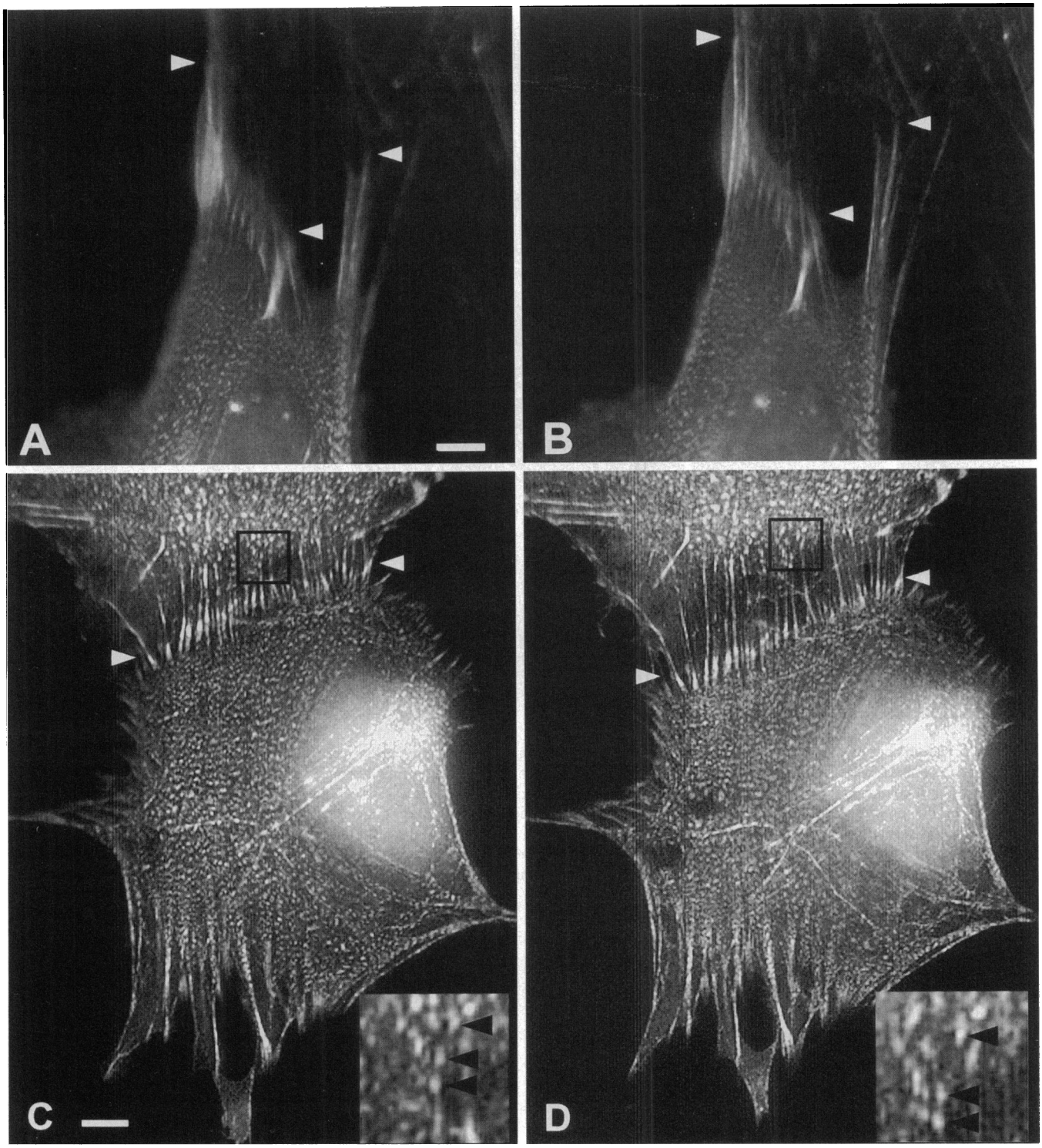

FIGURE 4 α-Actinin is concentrated at the tips of filament bundles along the protruding margin. (*A–D*) Time series of two pairs of SW3T3 cells that have been microinjected with AR-α-actinin. (*A*) and (*B*) The upper cell is contracting and the lower cell is protruding. Images shown were acquired 7 min apart. (*C*) and (*D*) The lower cell is contracting and the upper cell is protruding. Images shown were acquired 5 min apart. In addition to periodic decoration of stress fibers, α-actinin is concentrated at the distal ends of actin filament bundles at the protruding margin of the cell (*white arrowheads*). These α-actinin-containing structures translocate along with the protruding margin. Within the protruding region, α-actinin fluorescence is less intense and lacks obvious periodicity. Enlargements of boxed regions in *C* and *D* (*insets*) show that protrusion is accompanied by an increase in spacing between foci of α-actinin at the base of the protrusion (*black arrowheads*). Bars, 5 μm (*A*) and 10 μm (*C*).

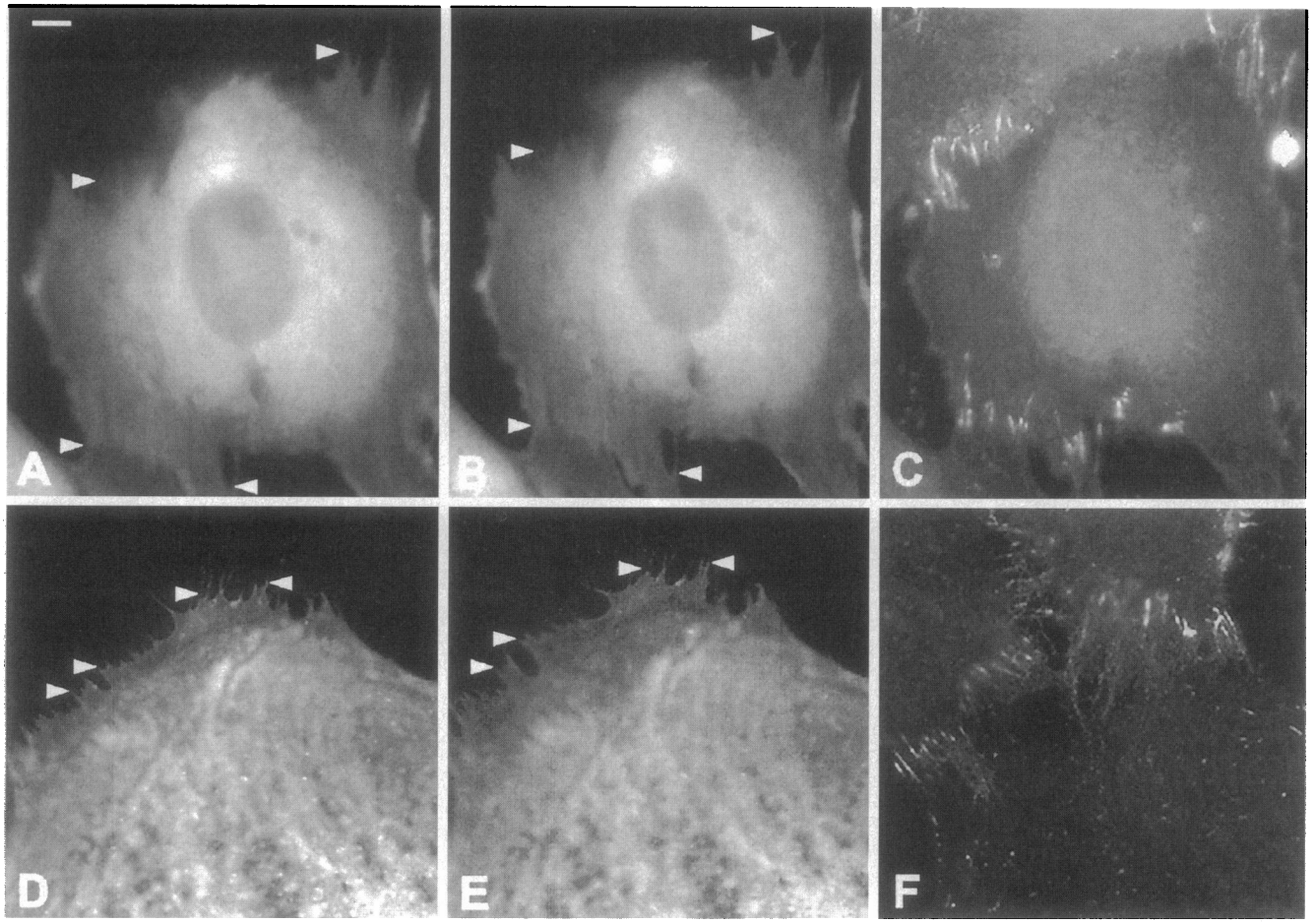

FIGURE 5 Protruding margins make adherens junctions with neighboring cells. Protruding cells were fixed and the localization of adherens junction proteins was examined by immunofluorescence. The first two images in each row are images from a time series of the protruding cell before fixation. The images in the last column are after fixation. (*A-C*) Localization of N-cadherin. Three minutes elapsed between *A* and *B*. This cell was protruding at two locations near the top of the image (*arrowheads*). N-cadherin is concentrated in discrete linear structures perpendicular to the protruding margins of the cell where it makes contact with a neighboring cell. Note that the protruding cell makes similar junctions with another cell at the lower left (*arrowheads*). The margin of this cell also protruded somewhat during the time lapse sequence. (*D–F*) Localization of β-catenin. Two minutes elapsed between *D* and *E*. The antigen is highly concentrated along the margin between the protruding cell and two neighbors in a pattern resembling N-cadherin localization. Bar, 5 μm.

along the axis of deformation was proportional to its initial distance from the baseline of the deformation (L_o; Fig. 6), suggesting that the deforming cytoplasm behaves as an integrated unit undergoing elastic stretch (Timoshenko and Young, 1968). Cytoplasmic strain ($\Delta L/L_o$) as a function of time for each protruding cell was well fit by Eq. 2; see Materials and Methods), which describes the time dependence of strain for a Kelvin-Voight viscoelastic solid. A plot of strain versus time for a representative cell is shown in Fig. 7 *A*. For all cells, the fits to the Kelvin-Voight model had R^2 values greater than 0.98 and χ^2 values less than 0.006. The combined data for six cells gave a mean limiting strain (σ/E) of 0.58 ± 0.135 SEM and a mean strain rate (E/η) of 4.3 ± 2.4 (SEM) × 10^{-3} s^{-1}. For data sets that included both the beginning and the end of a protrusion, σ/E was also calculated from direct measurements of the initial and final length of the protruding column of cytoplasm, giving a mean value of 0.445 ± 0.04 (SEM; n = 37). This is within the range of values obtained by fitting data to the Kelvin-Voight model. Very rarely (3 of >100 cells examined), a portion of the protruding cell margin was observed to become uncoupled from its contact with the neighboring cell and recoil along the axis of protrusion. Plots of strain versus time during the recoil of these cells also fit a Kelvin-Voight model, with a mean relaxation rate of 9.36 ± 3.2 (SEM) × 10^{-3} s^{-1} (Fig. 7 *B*).

Protrusion is not accompanied by commensurate changes in diameter

Additional information about the mechanical properties of a material can also be obtained by examining how its diameter changes as it elongates. We directly measured the length and width of extending portions of the cell in images taken at the beginning and the end of each time series. We

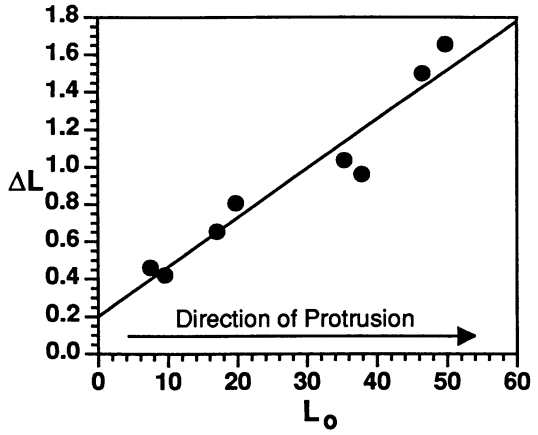

FIGURE 6 Displacement per unit time (ΔL) of markers is a linear function of initial distance along the axis of deformation from the baseline of extension (L_o). ΔL (μm) for a 1-min time interval is plotted versus L_o (μm) for beads and vesicles in the cell depicted in Fig. 2. The solid line was fit to the data by linear least squares. The R^2 value is 0.93. A linear relationship between ΔL and L_o is characteristic of elastic deformation.

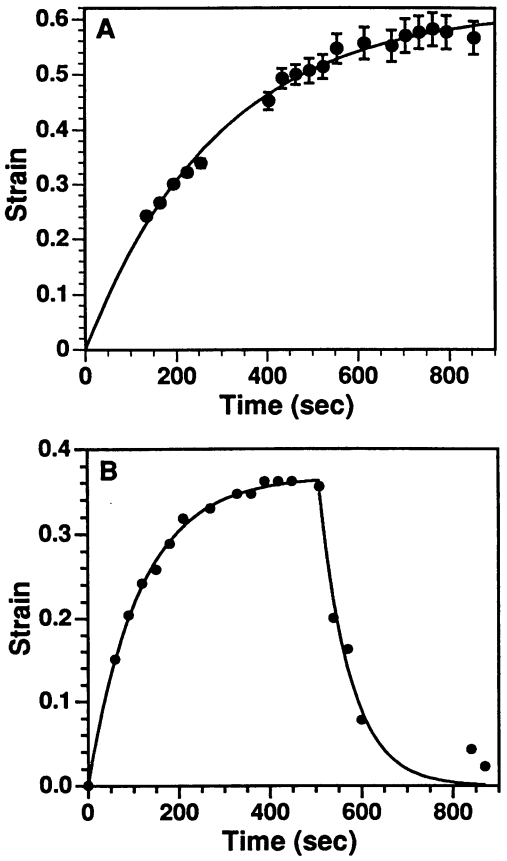

FIGURE 7 Strain is plotted with respect to time (sec) for two representative cells. Strains were calculated from ΔL and L_o. In cell A, the data points represent mean strain for multiple strain markers (beads and vesicles). In cell B, the time-dependent length of the protruding region from baseline to cell margin was used to calculate strain, as no beads or vesicles were present in the cytoplasm behind the portion of the cell margin that recoiled. The data were fit to Eq. 2 and renormalized as described in Materials and Methods. (*A*) The solid curve is the best fit of the renormalized data to Eq. 1, which describes the time dependence of strain for a Kelvin-Voight viscoelastic solid. The data fit the model with $R^2 = 0.99$, $\chi^2 = 0.002$. σ/E for this data set was 0.62. E/η was 3.4×10^{-3} s^{-1}. Error bars are standard error of the mean for all markers at each time point. (*B*) For this cell, which exhibited spontaneous recoil of the protruding margin, both the deformation and the recoil fit the Kelvin-Voight model with $R^2 = 0.99$ and 0.98, respectively. The rising curve gives $\sigma/E = 0.37$ and $E/\eta = 1.6 \times 10^{-2}$ s^{-1}. The curve fit to the relaxation gives $E/\eta = 8.8 \times 10^{-3}$ s^{-1}. The similarity of the deformation and the recoil suggest that the exponential rise in strain primarily reflects the properties of the deformed cell, rather than exponential variation in the contractile stress exerted by the neighboring cell.

estimated changes in height of the extending portion of the cell from the relative fluorescence intensity of the volume marker (10-kDa rhodamine-dextran), as by the Beer-Lambert relation the fluorescence intensity of a uniformly distributed probe is directly proportional to the path length. To correct for lamp variability and photobleaching, the intensity of rhodamine-dextran fluorescence in the extending region was normalized to the fluorescence intensity in a nondeforming portion of the same cell. In 80% of cells analyzed ($n = 13$), the extending part of the cell either did not change in diameter or expanded very slightly as it was stretched (Table 1). When fractional change in diameter was plotted against fractional change in length, it could be seen that significant decreases in diameter were associated only with the greatest changes in length, with an apparent threshold between 30 and 40% measured strain (Fig. 8). As most of the cells used for these measurements began extending before the time series was initiated or between acquisition of the first two images, the actual strain at which this threshold occurs is likely to be somewhat greater than 40%. Examination of intermediate images in the time series for the cases above this threshold showed that, in three of them, diameter was constant until the measured strain reached approximately 20 to 30% and then decreased rapidly. In the fourth case, diameter decreased continuously throughout the time series. This was also the case that exhibited the greatest total increase in length, so it may already have exceeded the threshold before the time series began.

DISCUSSION

Adherens junctions are widely assumed to play a role in the mechanical integration of tissues (Takeichi, 1995). They are a prominent morphological feature of endothelial and epithelial cell cultures. Adherens junctions between fibroblasts have received comparatively little attention in the literature, perhaps because fibroblasts are thought of as solitary cells that do not form a mechanically integrated tissue. Yet our data show that SW3T3 cells make contacts sufficient to withstand the tensile stresses exerted by a contracting cell on its neighbor and to transmit these stresses to the mechanically coupled cell, deforming it in the process. The junctions were observed even in subconfluent cultures, where contacts between fibroblasts typically are transient (Heaysman and Pegrum, 1973). The localization of junc-

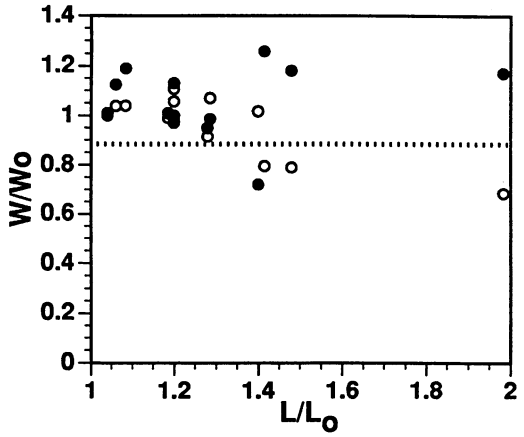

FIGURE 8 Plot of fractional changes in diameter (W/W_o) measured as width (○) or height (●) of each protrusion as a function of fractional change in length (L/L_o). Below a strain threshold of 0.3 to 0.4 (L/L_o = 1.3 to 1.4), narrowing of protrusions is negligible as they elongate ($W/W_o \geq 1$). Above the strain threshold, significant narrowing was observed in some cases. The dashed line demarcates one standard deviation below the mean value of W/W_o.

tional proteins in SW3T3 cells is similar to that recently reported for WI-38 fibroblasts, in which N-cadherin, α-actinin, and catenins were found to be associated with adherens junctions, whereas vinculin was relatively absent, as we also observed in this study (Knudson et al., 1995). This suggests that such junctions may be a common feature of cell-cell interactions between fibroblasts.

Analysis of cellular deformation in response to contractile stresses transmitted through these adherens junctions suggests that under these conditions the cytoplasm of Swiss 3T3 cells can be described as a simple Kelvin-Voight viscoelastic solid, in which a spring and a dashpot operate in parallel (Fig. 1 *B*). Similar models have been proposed to describe the mechanical properties of macrophages, of leukocytes undergoing small deformations, and of lamellipodial protrusions at the leading edge of migrating fibroblasts (Bizal et al., 1991; Chien et al., 1984; Felder and Elson, 1990). We note that in this study we are observing the mechanical properties of the cells at rates of deformation within a relatively limited range. Under other conditions, the viscoelastic response may differ depending on the characteristic times of the various modes of relaxation relative to the rate of deformation.

TABLE 1 Summary of mechanical properties of Swiss 3T3 cells under tension

σ/E	
From curve fitting	0.58 ± 0.135* (n = 6)
From direct measurement	0.445 ± 0.04* (n = 37)
E/η	4.3 ± 2.4 × 10^{-3} s^{-1}* (n = 6)
$(W_o - W)/\Delta L^{\dagger}$	
x–y plane	0.021 ± 0.024* (n = 13)
z axis	−0.041 ± 0.03* (n = 13)

*Mean ± standard error.

†W_o is initial diameter, W is final diameter, and ΔL is change in length. A positive value of this expression indicates a decrease in diameter and a negative value indicates an increase in diameter during elongation. For a closed system, this is known as the Poisson ratio.

In applying the Kelvin-Voight model to our data, we are making the assumptions that the stress applied by the contracting cell is constant over time and that the extent of contraction is determined by the elastic resistance of its neighbor. The observation that recoil, when it occurs, is essentially the reverse of deformation (Fig. 7 *B*) seems to support this assumption. However, because instances of spontaneous recoil were very rare, and because we were unable to induce recoil by a variety of methods reported to antagonize adherens junctions (EGTA, HAV peptide, and anti-cadherin antibodies), we do not have sufficient data to rule out definitively an alternative model in which the deformed cell is purely elastic, rather than viscoelastic, and the neighbor cell contracts auxotonically. In either case, the data suggest that cytoplasm is significantly elastic under physiological stress. The exponential time course of the protrusion we have observed distinguishes it from the protrusion of lamellipodia at the leading edge of a migrating fibroblast and during phagocytosis, for which the time course is linear (Evans et al., 1993; Felder and Elson, 1990).

Assuming that the Kelvin-Voight model is correct, if the magnitude of the stress exerted by the contracting cell were known, quantitative values for E and η could be calculated from our data. At present, we have no means of measuring the stress exerted by a single contracting fibroblast on a glass coverslip. However, several values exist in the literature for the stress exerted by cells undergoing contraction. A value of 10^5 dynes/cm^2 was recently reported for the isometric tension exerted by a population of fibroblasts contracting a collagen gel (Kolodney and Wysolmerski, 1992). Evans has reported a value of 10^4 dynes/cm^2 for the contractile stress exerted by a neutrophil during phagocytosis of a yeast (Evans et al., 1993). The contractile stress exerted by a fish keratocyte migrating on a silicon substratum has been measured to be 7×10^3 dynes/cm^2 (Lee et al., 1994). Unpublished data from another laboratory suggest that the stress exerted by contracting 3T3 cells is of similar magnitude (Michael P. Sheetz, personal communication). Assuming that the contracting cells in our system exert a constant stress of $\sim 10^4$ dynes/cm^2, we calculate mean values of $E = 1.7 \times 10^4$ dynes/cm^2 and $\eta = 4 \times 10^6$ Poise. These values are compared with values reported for other cell types in Table 2.

The identity of the elastic and viscous components responsible for the mechanical properties of SW3T3 fibroblasts remains to be determined. However, as the beads we are using as strain gauges are located within the cytoplasm, the proportionality we observed between ΔL and L_o clearly indicates that the elastic component resides in the cytoplasm itself. It has been proposed that cytoplasm may be a composite material reflecting the viscoelastic properties of an integrated network of microtubules, intermediate filaments, and actin filaments (Janmey et al., 1991). In support of this hypothesis, drugs that depolymerize cytoskeletal filaments

TABLE 2 Selected literature values for E and η of cytoplasm*

Specimen	E (dynes/cm^2)	η (Poise)	Reference
Swiss 3T3 cells	1.7×10^4	4×10^6	This study
Squid axoplasm	$10^3 - 10^5$	$10^5 - 10^6$	Sato et al., 1984
Macrophages	~150	2.5×10^4	Zaner and Valberg, 1989
	ND	$1.5 - 4.5 \times 10^3$	Bizal et al., 1991
Macrophage extracts	$1 - 3 \times 10^4$	ND	Janmey et al., 1994
Leukocytes	≤500	130	Schmid-Schonbein et al., 1981
Platelets	$10^4 - 5 \times 10^5$	Very low	Radmacher et al., 1996

*Variety of shear rates and shear stresses.

are reported to abolish cellular elasticity (e.g., Tsai et al., 1994; Wang et al., 1993a,b). The apparent elongation of actin filament bundles during deformation raises the additional possibility that the actin filament bundles themselves may be elastic like myofibrils in skeletal muscle (Wang et al., 1993a,b), although other possible mechanisms for elongation such as addition of actin monomers or filament sliding cannot be ruled out. The viscous component could reflect the viscosity of cytoplasm, the viscosity of the cell membrane, a variable rate of contraction by the pulling cell (if the contraction is auxotonic), or some combination of these parameters (Elson, 1988).

Narrowing of protrusions was negligible below a strain threshold of ~0.4. Thus, protrusion results in a local increase in cell volume. For the cell in Fig. 2, we calculate that the increase in volume was ~28%. The increase in volume might involve local uptake of extracellular water or it might be compensated for by small decreases in volume spread out over the rest of the cell. If the extending portion of the cell represents ≤10% of total cell volume, then the volume of the rest of the cell would have to decrease by only ≤3% to maintain constant volume. If there is no uptake of water during elongation, this would suggest that the Poisson ratio of cytoplasm in fibroblasts is near zero or negative under these conditions. Negative Poisson ratio is an unusual feature of some networks or of composite media consisting of a network embedded in a material with a positive Poisson ratio (Boal et al., 1993; Nkansah et al., 1993). Such materials have a high shear modulus, making them especially resistant to shearing stress. In this context, the rapid decrease in diameter above the threshold strain might reflect collapse of the structure responsible for the negative Poisson ratio.

On the other hand, stretching during protrusion may increase the water permeability of the plasma membrane, resulting in a net increase in cellular volume. Another possible consequence of the increase in membrane tension associated with cellular deformation might be alteration of the open probability of stretch-activated ion channels, leading to the activation of signaling pathways and eventually even modifying gene expression (Sackin, 1995). Mechanotransduction of transcellular stresses to the nucleus through the cytoskeleton might also modify gene expression (Ingber et al., 1994). These possibilities remain to be investigated.

Throughout our analysis we have treated the cytoplasmic compartment marked by microinjected beads as a uniform material on the basis that markers with the same L_o kept abreast of one another during the deformation and that the strains we observed for all markers within a given column of extending cytoplasm were the same within experimental error. A simple model for our data is that our markers are entrapped in a three-dimensional network of cytoskeletal filaments attached to or continuous with the actin fiber bundles that insert into adherens junctions at points of contact or overlap between adjacent fibroblasts. In response to contractile stress transmitted through the adherens junctions, the actin filament bundles elongate, stretching the attached gel network and dragging the entrapped markers along with it (Fig. 1 *A*).

Our data make it clear that mechanical coupling between fibroblasts and the viscoelastic response of the cells to tensile stress are factors that must be taken into account in constructing biomechanical models of wound closure or extracellular matrix remodeling by fibroblasts. As our measurements were made in cells responding to stresses of physiological magnitude, it seems likely that a Kelvin-Voight element will adequately represent the mechanical behavior of fibroblasts during these important biological processes. In addition, the experimental system we have described can be used to investigate the mechanical properties of other cell types, to examine the regulation of cellular mechanical properties, and to elucidate the role of the various cytoskeletal filaments in determining these properties.

We gratefully acknowledge Drs. Vladislav Markin, Robert Wysolmerski, Margaret Wheelock, and Mike Sheetz for very helpful advice and discussion. We also thank Drs. Paul Janmey, Kris Kamm, and Helen Yin for critical reading of the manuscript at various stages. We thank Dr. Margaret Wheelock for the generous gift of monoclonal antibody to N-cadherin. This work was supported by National Science Foundation grant MCB-9304603 and American Heart grant-in-aid 93011130 to Dr. Luby-Phelps.

REFERENCES

Beckerle, M. C. 1984. Microinjected fluorescent polystyrene beads exhibit saltatory motion in tissue culture cells. *J. Cell Biol.* 98:2126–2132.

Bizal, C. L., J. P. Butler, and P. A. Valberg. 1991. Viscoelastic and motile properties of hamster lung and peritoneal macrophages. *J. Leukocyte Biol.* 50:240–251.

Boal, D. H., U. Seifert, and J. C. Shillcock. 1993. Negative Poisson ratio in two-dimensional networks under tension. *Phys. Rev. E.* 48: 4274–4283.

Chien, S., G. W. Schmid-Schonbein, K. L. Sung, E. A. Schmalzer, and R. Skalak. 1984. Viscoelastic properties of leukocytes. *Kroc Found. Ser.* 16:19–51.

Danowski, B. A., and A. K. Harris. 1988. Changes in fibroblast contractility, morphology, and adhesion in response to a phorbol ester tumor promoter. *Exp. Cell Res.* 177:47–59.

DeBiasio, R., G. R. Bright, L. A. Ernst, A. S. Waggoner, and D. L. Taylor. 1987. Five-parameter fluorescence imaging: wound healing of living Swiss 3T3 cells. *J. Cell Biol.* 105:1613–1622.

Elson, E. L. 1988. Cellular mechanics as an indicator of cytoskeletal structure and function. *Annu. Rev. Biophys. Biophys. Chem.* 17: 397–430.

Evans, E., A. Leung, and D. Zhelev. 1993. Synchrony of cell spreading and contraction force as phagocytes engulf large pathogens. *J. Cell Biol.* 122:1295–1300.

Felder, S., and E. Elson. 1990. Mechanics of fibroblast locomotion: quantitative analysis of forces and motions at the leading lamellas of fibroblasts. *J. Cell Biol.* 111:2513–2526.

Feramisco, J. R. 1979. Microinjection of fluorescently labeled α-actinin into living fibroblasts. *Proc. Natl. Acad. Sci. U.S.A.* 76:3967–3971.

Feramisco, J. R., and K. Burridge. 1980. A Rapid purification of α-actinin, filamin, and a 130,000-dalton protein from smooth muscle. *J. Biol. Chem.* 255:1194–1199.

Geerts, H., M. De Brabander, R. Nuydens, S. Geuens, M. Moeremans, J. De Mey, and P. Hollenbeck. 1987. Nanovid tracking: a new automatic method for the study of mobility in living cells based on colloidal gold and video microscopy. *Biophys. J.* 52:775–782.

Heaysman, J. E. M., and S. M. Pegrum. 1973. Early contacts between fibroblasts. *Exp. Cell Res.* 78:71–78.

Hiramoto, Y. 1990. Mechanical properties of the cortex before and during cleavage. *Ann. N.Y. Acad. Sci.* 582:22–30.

Ingber, D. E., L. Dike, L. Hansen, S. Karp, H. Liley, A. Maniotis, H. McNamee, D. Mooney, G. Plopper, and J. Sims. 1994. Cellular tensegrity: exploring how mechanical changes in the cytoskeleton regulate cell growth, migration, and tissue pattern during morphogenesis. *Int. Rev. Cytol.* 150:173–224.

Janmey, P. A., U. Euteneuer, P. Traub, and M. Schliwa. 1991. Viscoelastic properties of vimentin compared with other filamentous biopolymer networks. *J. Cell Biol.* 113:155–160.

Janmey, P. A., S. Hvidt, J. Kas, D. Lerche, A. Maggs, E. Sackmann, M. Schliwa, and T. P. Stossel. 1994. The mechanical properties of actin gels: elastic modulus and filament motions. *J. Biol. Chem.* 269: 32503–32513.

Knudson, K. A., A. P. Soler, K. R. Johnson, and M. J. Wheelock. 1995. Interaction of α-actinin with the cadherin/catenin cell-cell adhesion complex via α-catenin. *J. Cell Biol.* 130:67–77.

Kolodney, M. S., and R. B. Wysolmerski. 1992. Isometric contraction by fibroblasts and endothelial cells in tissue culture: a quantitative study. *J. Cell Biol.* 117:73–82.

Lee, J., M. Leonard, T. Oliver, A. Ishihara, and K. Jacobson. 1994. Traction forces generated by locomoting keratocytes. *J. Cell Biol.* 127: 1957–1964.

Liu, Z. Y., J. I. Young, and E. L. Elson. 1987. Rat basophilic leukemia cells stiffen when they secrete. *J. Cell Biol.* 105:2933–2943.

Meigs, J. B., and Y. Wang. 1986. Reorganization of α-actinin and vinculin induced by a phorbol ester in living cells. *J. Cell Biol.* 102:1430–1438.

Nkansah, M. A., K. E. Evans, and J. Hutchinson. 1993. Modelling the effects of negative Poisson's ratios in continuous-fibre composites. *J. Mater. Sci.* 28:2687–2692.

Provance, D. W., A. MacDowall, M. Marko, and K. Luby-Phelps. 1993. Cytoarchitecture of size-excluding compartments in living cells. *J. Cell Sci.* 106:565–578.

Qian, H., M. P. Sheetz, and E. L. Elson. 1991. Single particle tracking: analysis of diffusion and flow in two-dimensional systems. *Biophys. J.* 60:910–921.

Radmacher, M., M. Fritz, C. M. Kacher, J. P. Cleveland, and P. K. Hansma. 1996. Measuring the viscoelastic properties of human platelets with the atomic force microscope. *Biophys. J.* 70:556–567.

Sackin, H. 1995. Stretch-activated ion channels. *Kidney Int.* 48: 1134–1147.

Sanger, J. M., B. Mittal, M. B. Pochapin, and J. W. Sanger. 1986. Myofibrillogenesis in living cells microinjected with fluorescently labeled α-actinin. *J. Cell Biol.* 102:2053–2066.

Sato, M., T. Z. Wong, D. T. Brown, and R. D. Allen. 1984. Rheological properties of living cytoplasm: a preliminary investigation of squid axoplasm (*Loligo pealei*). *Cell Motil. Cytoskeleton.* 4:7–23.

Schmid-Schonbein, G. W., K. L. Sung, H. Tozeren, R. Skalak, and S. Chien. 1981. Passive mechanical properties of human leukocytes. *Biophys. J.* 36:243–256.

Simon, S. I., and G. W. Schmid-Schonbein. 1990. Kinematics of cytoplasmic deformation in neutrophils during active motion. *J. Biomech. Eng.* 112:303–310.

Spudich, J. A., and S. Watt. 1971. The regulation of rabbit skeletal muscle contraction. *J. Biol. Chem.* 246:4866–4871.

Takeichi, M. 1995. Morphogenetic roles of classic cadherins. *Curr. Opin. Cell Biol.* 7:619–627.

Timoshenko, S., and D. H. Young. 1968. Elements of Strength of Materials. Van Nostrand, New York. 377 pp.

Tsai, M. A., R. S. Frank, and R. E. Waugh. 1994. Passive mechanical behavior of human neutrophils: effect of cytochalasin B. *Biophys. J.* 66:2166–2172.

Wadsworth, P. 1987. Microinjected carboxylated beads move predominantly poleward in sea urchin eggs. *Cell Motil. Cytoskeleton.* 8:293–301.

Wang, N., J. P. Butler, and D. E. Ingber. 1993a. Mechanotransduction across the cell surface and through the cytoskeleton. *Science.* 260: 1124–1127.

Wang, K., R. McCarter, J. Wright, J. Beverly, and R. Ramirez-Mitchell. 1993b. Viscoelasticity of the sarcomere matrix of skeletal muscles. The titin-myosin composite filament is a dual-stage molecular spring. *Biophys. J.* 64:1161–1177.

Zahalak, G. I., W. B. McConnaughey, and E. L. Elson. 1990. Determination of cellular mechanical properties by cell poking, with an application to leukocytes. *J. Biomech. Eng.* 112:283–294.

Zaner, K. S., and P. A. Valberg. 1989. Viscoelasticity of F-actin measured with magnetic microparticles. *J. Cell Biol.* 109:2233–2243.